Drastic enhancement of the Raman intensity in few-layer InSe by uniaxial strain

Chaoyu Song,[1,3,*] Fengren Fan,[1,2,3,*] Ningning Xuan,[4,*] Shenyang Huang,[1,3] Chong Wang,[1,3] Guowei Zhang,[1,3] Fanjie Wang,[1,3] Qiaoxia Xing,[1,3] Yuchen Lei,[1,3] Zhengzong Sun,[4,†] Hua Wu,[1,2,3,‡] and Hugen Yan[1,3,§]

[1]*State Key Laboratory of Applied Surface Physics and Department of Physics, Fudan University, Shanghai 200433, China*
[2]*Key Laboratory of Computational Physical Sciences (Ministry of Education), Fudan University, Shanghai 200433, China*
[3]*Collaborative Innovation Center of Advanced Microstructures, Nanjing 210093, China*
[4]*Department of Chemistry and Shanghai Key Laboratory of Molecular Catalysis and Innovative Materials, Fudan University, Shanghai 200433, China*

(Received 21 March 2019; published 10 May 2019)

The vibrational and electronic properties of two-dimensional (2D) materials can be efficiently tuned by external strain due to their good stretchability. Resonant Raman spectroscopy is a versatile tool to study the physics of phonons, electrons, and their interactions simultaneously, which is particularly useful for the investigation of strain effect on 2D materials. We report the resonant Raman study of strained few-layer InSe (γ phase). Under $\sim$1% of uniaxial tensile strain, one order of magnitude enhancement of Raman intensity for the longitudinal optical (LO) phonon is observed, while other modes exhibit only modest change. Further analysis demonstrates that it arises from the intraband electron-phonon scattering channel for a LO phonon in resonance. The large enhancement of Raman intensity provides us with a sensitive method to characterize the strain effect, and a mapping of the strain distribution in a wrinkled sample is demonstrated. In addition, we observe sizable redshifts of first-order optical phonon modes. The shift rate exhibits phonon-mode dependence, in excellent agreement with density functional perturbation theory calculations. Our study paves the way for sensitive strain quantification in few-layer InSe and its application in flexible electronic and optoelectronic devices.

DOI: 10.1103/PhysRevB.99.195414

I. INTRODUCTION

The mechanical cleavage of graphene [1] by Novoselov *et al.* has aroused tremendous research interest in two-dimensional (2D) materials. A variety of 2D semimetals and semiconductors has been discovered ever since, such as transition-metal dichalcogenides (TMDCs) [2], silicene [3], stanine [4], and black phosphorus [5,6]. Atomically thin indium selenide (γ phase) has joined the family lately with unique electronic properties [7–9]. The quantum Hall effect was observed in the high-quality few-layer InSe electronic devices [9]. Strong quantum confinement in the out-of-plane direction gives rise to a layer-dependent band gap [7], covering a large range of visible and near-infrared regions. Few-layer InSe has promised great application potentials in electronics and optoelectronics [10–12].

The mechanical stretchability of 2D materials opens the door for straining, to continuously and reversibly tune their lattice constants and electronic properties [13]. Raman spectroscopy is a crucial diagnostic tool to evaluate the strain effect. Phonon softening and splitting are commonly observed in 2D materials under uniaxial tensile strain, such as graphene [14,15], TMDCs [16,17], and black phosphorus [18,19], indicating the weakening of the bond strength and the symmetry breaking. The band structure and electronic properties of 2D materials can be engineered efficiently via strain as well. For example, the prominent strain-induced shift of the band gap and indirect-to-direct band-gap transition were observed in multilayer TMDCs [20]. Owing to the small Young's modulus ($\sim$45 N/m) [21], the band gap of few-layer InSe can be easily tuned by uniaxial tensile strain with shift rate up to 90–150 meV/% [22,23]. Therefore, few-layer InSe, with largely strain-tunable band gaps, exhibits great application potentials in flexible and wearable electronics. It calls for a comprehensive understanding of lattice vibrations and their interactions with electrons in strained InSe.

In this work, we performed resonant Raman spectroscopy to study the vibrational and electronic properties of few-layer InSe (γ phase) under uniaxial tensile strain. Here we particularly focus on the Raman intensity, in contrast to previous similar studies on other 2D materials in which the Raman intensity typically did not notably change under strain and little attention was paid to it. The energy match between photons and electronic intermediate states (exciton or continuum bands) provides us abundant information on the band structures and electronic properties, in addition to the phonon physics [24]. Combing the merits of tunable strain and resonant Raman spectroscopy, we are able to measure the Raman spectra of few-layer InSe under resonant and near-resonant conditions with a single 514.5 nm laser. Drastic enhancement of the Raman intensity of the A_1 (Γ_1^1)-LO and E (Γ_3^1)-LO phonon modes is observed in the process of applying uniaxial tensile strain from zero to 1.15%, while that for other Raman modes only changes modestly. This is ascribed to the intraband electron-phonon scattering channel for a

*These authors contributed equally to this work.
†zhengzong_sun@fudan.edu.cn
‡wuh@fudan.edu.cn
§hgyan@fudan.edu.cn

longitudinal-optical (LO) phonon in resonance. In addition, sizable redshifts are observed for first-order phonon modes located in the range of 100–300 cm^{-1}. Furthermore, as a proof of concept, we determine the spatial variation of strain in a wrinkled few-layer InSe flake by mapping the Raman intensity of the A_1 (Γ_1^1)-LO phonon.

II. EXPERIMENTAL METHODS

Few-layer InSe was exfoliated from bulk crystal of InSe (2D Semiconductors Inc.) onto polydimethylsiloxane (PDMS) substrates by the Scotch-tape method [1]. The flakes were subsequently transferred to flexible poly(ethylene terephthalate)-glycol (PETG) substrates with thickness of 0.3 mm. The thickness of InSe was determined by optical contrast and further verified by atomic force microscope (AFM) and photoluminescence (PL) spectroscopy (see the Supplemental Material (SM), Sec. S1 [25]). The wrinkled InSe was fabricated by the conventional method of elongating and releasing flexible substrate [26,27]. The PDMS substrate (1 mm thick) was first prestretched by 50–100%. Then InSe flakes were deposited. The PDMS substrate was then released suddenly, creating wrinkles in few-layer InSe (see SM, Sec. S10 [25]). The topography of the wrinkles was measured by Bruker Dimension Edge AFM (probe model RTESP-300, tapping mode).

Resonant Raman spectra were taken by a Horriba HR800 Raman system with the excitation of 514.5 nm laser (spot size ~1 μm, laser power of 50 μW). The incident laser was focused by a 100 × (NA = 0.9) objective. The PL measurement was performed by the same setup with a 473 nm laser (spot size ~1 μm, laser power of 500 μW) for excitation. The laser power was kept low enough to prevent potential damage to the samples. The differential reflectance spectra were taken by an Andor SR500i spectrometer in conjunction with a Nikon Eclipse Ti microscope equipped with a 50 × (NA = 0.7) objective. All experiments reported in this paper were conducted at room temperature.

III. RESULTS AND DISCUSSION

A. The vibrational properties of unstrained few-layer InSe

InSe (γ-phase) crystal has a layered hexagonal structure, as depicted in Fig. 1(a). In each layer, the lattice consists of four atomic planes arranged in the sequence of Se-In-In-Se. Individual layers are held together by van der Waals forces. Few-layer InSe (γ phase) belongs to point group C_{3v}, and the normal modes of the vibrations are $4A_1$ (Γ_1) + $4E$ (Γ_3). Among them, one A_1 mode and one E mode are acoustic, while the remaining modes are optical (all both infrared and Raman active) [28]. The vibrations are illustrated in Fig. 1(b). Figure 1(c) shows Raman spectra of unstrained 3-, 10-, 30-layer, and bulk InSe with the excitation of a 514.5 nm laser. The E (Γ_3^2) mode is beyond the lower limit of our setup, and hence not discussed here. Five Raman peaks are observed in the range of 100–300 cm^{-1}. They are A_1 (Γ_1^2) at 115 cm^{-1}, E (Γ_3^3)/E (Γ_3^1)-TO at 178 cm^{-1} (TO is transverse optical phonon), A_1 (Γ_1^1)-TO at 196 cm^{-1}, A_1 (Γ_1^1)-LO at 199 cm^{-1}, and A_1 (Γ_1^3) at 227 cm^{-1}, respectively. All Raman spectra reported in this work are measured by backscattering geometry. The A_1 (Γ_1^1)-LO and E (Γ_3^1)-LO modes are forbidden or extremely weak by selection rules in such geometry [29–31], and hence not observed in off-resonant conditions with the excitation of 532 nm (see SM, Sec. S5 [25]) and 633 nm lasers [11]. However, the intensity of Raman scattering, especially for the forbidden modes, is enhanced if the energy of the incident photon (514.5 nm, 2.41 eV) is close enough to that of the B transition, which is the electronic transition between the top of the Se-4$p_{x/y}$ orbital band and the bottom of the conduction band (In-5s orbital) [32]. Therefore, we could observe a weak peak originated from the A_1 (Γ_1^1)-LO phonon mode, as shown in Fig. 1(c).

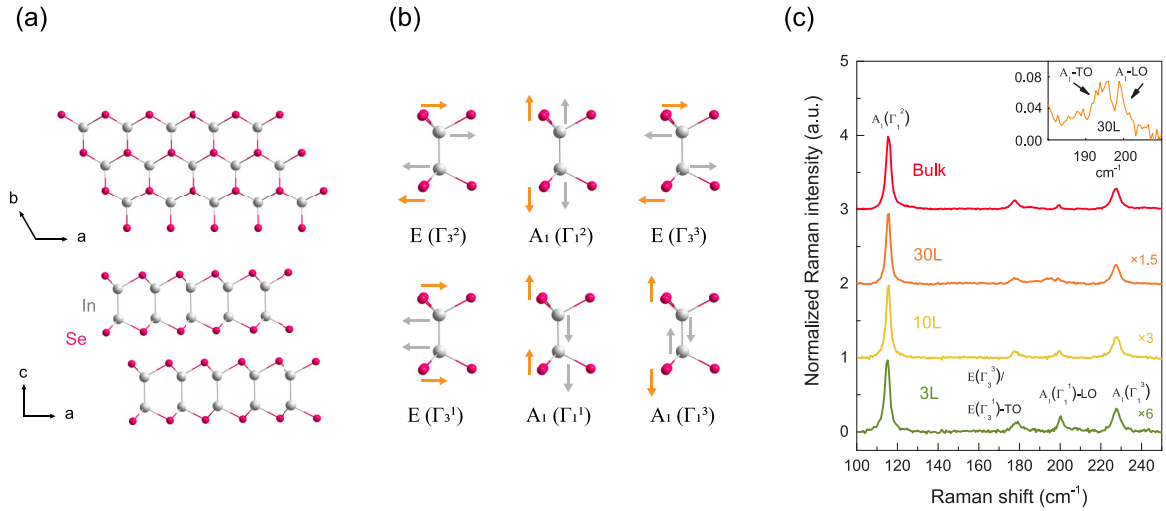

FIG. 1. (a) Crystal structures of monolayer InSe viewed from the c-axis direction (top) and of bilayer InSe viewed from the b-axis direction (bottom). (b) Lattice vibrations of all first-order optical phonon modes. Mulliken symbols are used in this work, while the corresponding Γ symbols are labeled in parentheses for comparison. (c) Raman spectra of 3-layer, 10-layer, 30-layer, and bulk InSe under no strain with the excitation of a 514.5 nm laser. The inset shows the zoom-in of the spectra near 200 cm^{-1} for the 30-layer InSe. The spectrum intensity is multiplied by a factor indicated beside each spectrum for 3 L, 10 L, and 30 L.

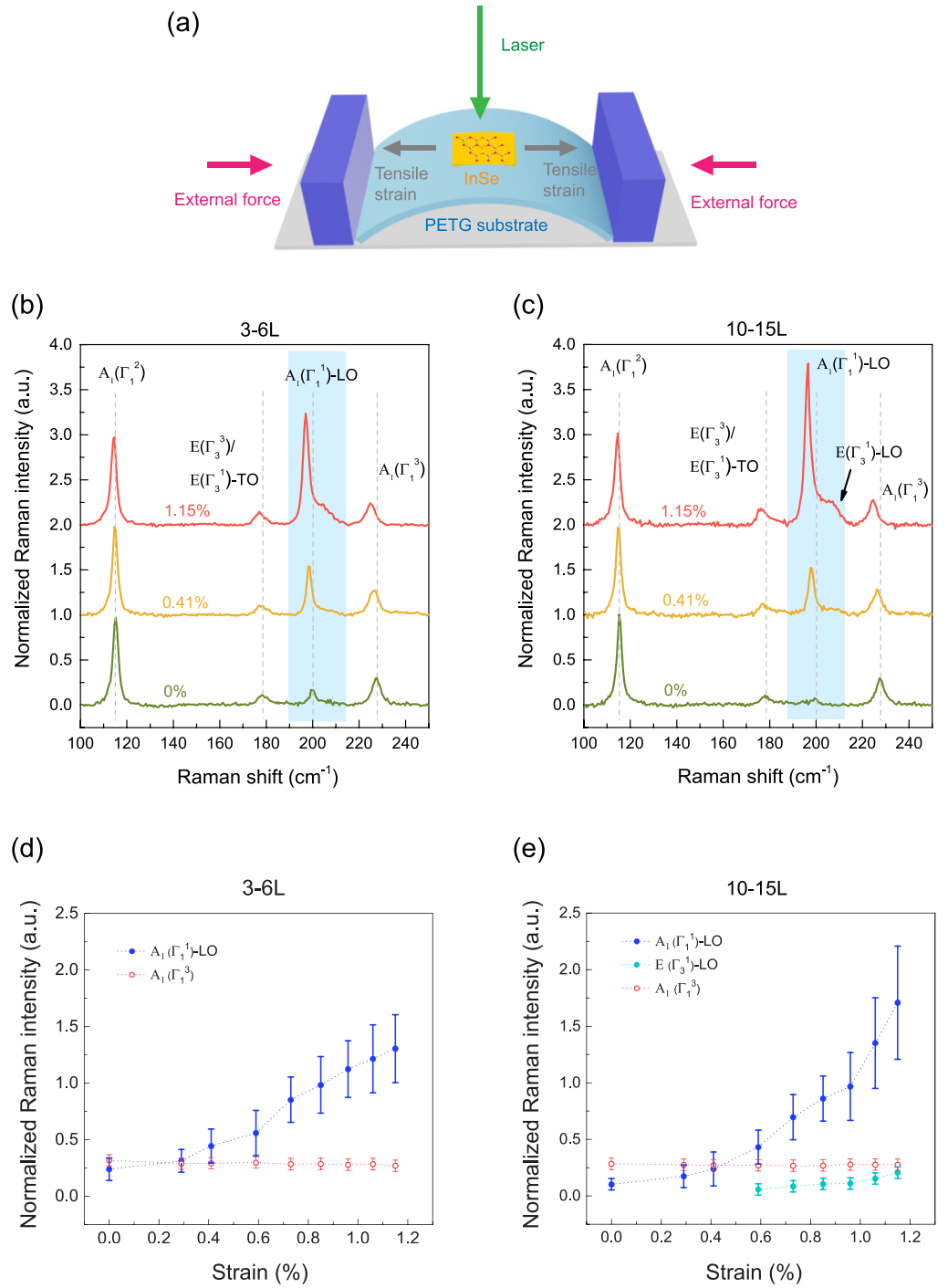

FIG. 2. (a) Schematic illustration of the two-point bending apparatus. Raman spectra of (b) 3–6 layer and (c) 10–15 layer InSe as uniaxial tensile strain is applied from zero to 1.15%. The assignment of the corresponding phonon mode for each Raman peak is marked. The blue rectangles highlight the enhanced LO phonon mode, and the vertical gray dashed lines indicate the positions of the respective Raman peaks under no strain. (d),(e) Normalized Raman intensity of enhanced LO modes and selection-rule-allowed A_1 (Γ_1^3) mode for 3–6 layer and 10–15 layer InSe, respectively, as a function of strain.

B. Giant enhancement of the Raman intensities of LO phonons

Uniaxial tensile strain was applied to few-layer InSe by a two-point bending scheme, as shown in Fig. 2(a). Flexible poly(ethylene terephthalate)-glycol (PETG) substrate was chosen, such that a minimal background signal was from the substrate itself. The strain in the stretch direction is determined according to the deflection of PETG substrates [20] (see SM, Sec. S2 [25]), and the strain along the other direction is ignored in the analysis. The comparison of strain effect without and with clamping shows that there is no sliding in InSe due to the good stretchability of the sample (see SM, Sec. S12 [25]). Therefore, clamping is not necessary for our study with moderate strain values.

We systematically measured the evolution of the resonant Raman spectra of few-layer InSe under uniaxial tensile strain. Two major strain effects are observed. One is the large enhancement of A_1 (Γ_1^1)-LO and E (Γ_3^1)-LO phonon modes, and the other is the sizable redshift of all first-order Raman modes. We categorize our samples into two groups with thickness of 3–6 layers and 10–15 layers according to the different enhancement magnitude, as shown in Figs. 2(b) and 2(c). It is worth noting, however, that all first-order phonon modes should exhibit enhancement in resonance conditions [29], but the enhancement of the A_1 (Γ_1^1)-LO and E (Γ_3^1)-LO modes is one order of magnitude larger than that of the other modes. Therefore, in this work, we mainly focus on the abnormally large enhancement of those two modes, and all spectra in Figs. 2(b) and 2(c) are normalized to have the same intensity for the A_1 (Γ_1^2) mode. As shown in Figs. 2(b) and 2(c), the intensity of the A_1 (Γ_1^1)-LO mode increases dramatically when uniaxial tensile strain is applied from zero to 1.15%. For 10–15-layer InSe, a broad shoulder simultaneously emerges at the high-energy side of the A_1 (Γ_1^1)-LO Raman peak, which is assigned to the E (Γ_3^1)-LO mode [28].

By fitting the spectra with the Lorenz formula, we obtain the intensity, frequency, and width of each Raman peak. Figures 2(d) and 2(e) show the evolution of normalized intensity of the enhanced phonon modes as uniaxial tensile strain is applied. The data points and error bars are based on the measurements of more than 10 samples for each group. For comparison, the normalized intensity of the A_1 (Γ_1^3) mode is also plotted. The normalized intensity of the A_1 (Γ_1^3) mode almost remains a constant, showing that the ratio of the Raman intensity of A_1 (Γ_1^3) to A_1 (Γ_1^2) is the same in the process of applying strain. Therefore, these selection-rule-allowed phonon modes exhibit a similar modest enhancement factor, which behaves quite differently from the forbidden LO phonon modes. We use the enhancement ratio $\alpha = \frac{I(\text{with 1.15\% tensile strain})}{I(\text{without strain})}$, which is the ratio of the normalized Raman intensity under 1.15% tensile strain to that without strain, to quantify the enhancement magnitude. For 3–6-layer InSe, the enhancement ratio α of A_1 (Γ_1^1)-LO is 5 ± 1. For 10–15-layer InSe, the enhancement effect becomes even more pronounced, with the enhancement ratio α of 18 ± 4. The Raman peak of the E (Γ_3^1)-LO mode is absent without strain, and gradually emerges with strain $>0.6\%$. By assuming that the intensity of the E (Γ_3^1)-LO mode without strain is at the same level of the spectrum background, a conservative estimation gives the enhancement ratio α of over 10.

C. Enhancing Raman intensities by intraband electron-phonon scattering channel

It is well known that the intensity of Raman scattering is enhanced under resonance conditions [24]. For few-layer InSe, the strain-induced modification of the band structure [22,23] evokes the change of resonant conditions when the excitation laser wavelength is fixed. As shown in Fig. 3(a), when uniaxial tensile strain is applied, the energy of the B transition shifts closer to that of the incident photon (514.5 nm, 2.41 eV) and, eventually, the intermediate electron/hole state changes from a virtual to a real energy state, so the Raman intensity exhibits enhancement. PL measurements were performed to quantitatively illustrate the strain effect on the band structures. The position of the PL peaks corresponds to the energy of the exciton, which is slightly smaller than the energy of the quasiparticle electronic transition, with the difference as the exciton binding energy [33]. The electronic intermediate state of resonant Raman scattering of few-layer InSe is the exciton state associated with the B transition (we call it exciton B for simplicity). Figure 3(b) shows the PL spectra of a strained 12-layer InSe; the peak shifts from 2.46 eV to approximately 2.41 eV as uniaxial tensile strain is applied from zero to 1.15%. Therefore, the resonance conditions are gradually satisfied. For few-layer InSe, the strain effect on the B transition is almost the same, all exhibiting a similar shift rate of $(45 \pm 10)\,\text{meV}/\%$ according to the PL spectra of strained 8 layer and 30 layer (see SM, Sec. S6 [25]). From the above argument, it is apparent that such enhancement of Raman intensity should be laser-wavelength dependent. If the laser energy is above the B transition, tensile strain will separate them further and no enhancement is supposed to occur. Indeed, this is the case for the excitation with a 473 nm laser, as shown in the SM, Sec. S4 [25]. In addition, we used a 488 nm laser (2.54 eV) to excite Raman scattering of a four-layer InSe, whose B-transition energy is approximately 2.53 eV, and a resonance effect was observed as illustrated in the SM, Sec. S11 [25].

The enhancement shows certain layer dependence as well, since the B-transition energy depends on the sample thickness. The different enhancement ratio between 3–6 layer and 10–15 layer InSe is consistent with this scenario. Figure 3(c) shows the differential reflectance spectra, $\frac{\Delta R}{R} = \frac{R_{\text{sample}} - R_{\text{substrate}}}{R_{\text{substrate}}}$, of one-layer to eight-layer InSe; the bump position (indicated by triangles) of the differential reflectance corresponds to exciton B [2]. Strong interlayer interactions give rise to prominent layer-dependent energy of exciton B, which is 2.47 eV for eight layers and increases to about 2.81 eV for a monolayer (without strain). Combing with the results of PL measurements, we summarize the layer- and strain-dependent energy of the exciton B in Fig. 3(d). It qualitatively explains why the 10–15-layer InSe exhibits larger resonant effect than the 3–6-layer InSe. The energy of exciton B is around 2.45–2.47 eV for 10–15 layers without strain, and 1.15% uniaxial tensile strain makes it redshift by 50 meV, in perfect match with the incident photon energy, while for unstrained 3–6-layer InSe, the energy of exciton B is about 2.50–2.55 eV. Therefore, tensile strain will make the resonant effect enhanced but still away from the optimum even for maximal strain (1.15%, redshift of $\sim$50 meV).

The enhancement depends on the phonon-mode character. Contrary to the conventional resonant Raman scattering that all phonon modes are enhanced on the same footing, herein we only observe a drastic enhancement of A_1 (Γ_1^1)-LO and E (Γ_3^1)-LO modes, while the enhancement of other phonon modes is much less significant by contrast. The larger enhancement of LO modes arises from the dominant intraband Fröhlich electron-phonon interactions near the resonance, which is originated from the scattering of electron or hole within the same band by the macroscopic electric field of an LO phonon [24]. According to Fermi's golden rule, the cross

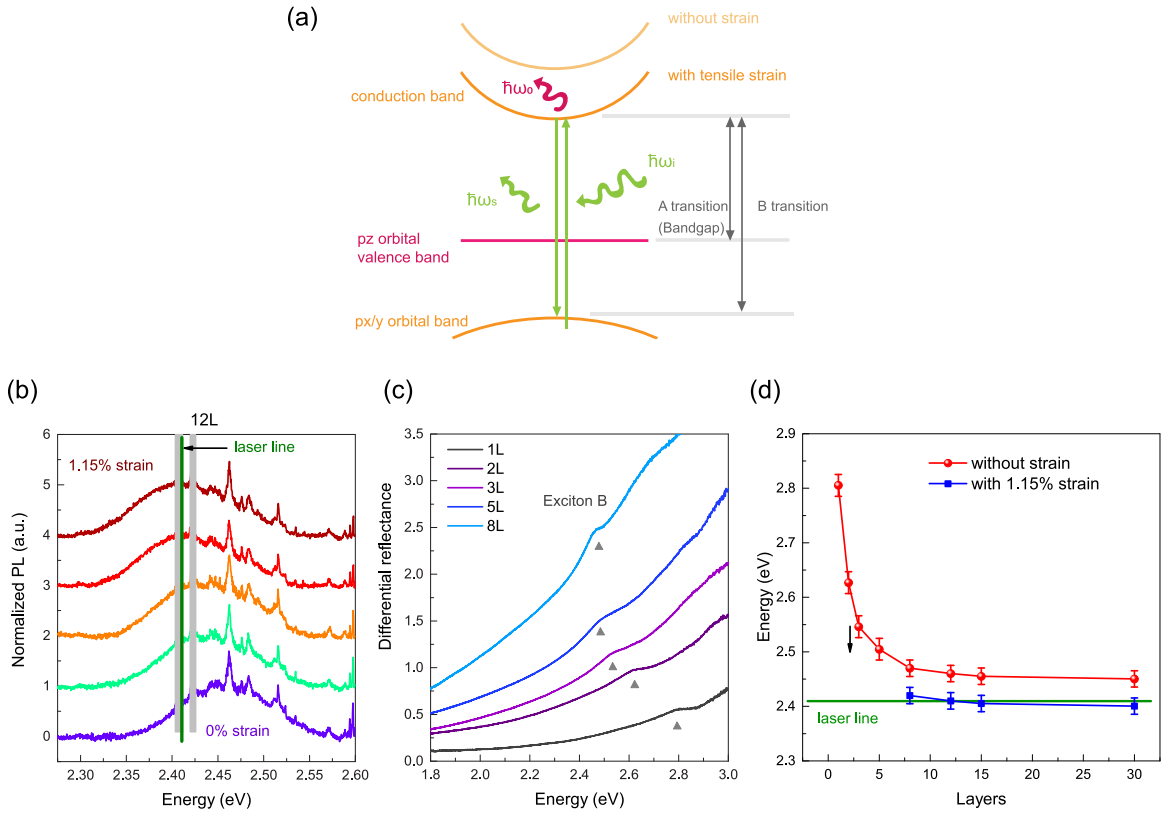

FIG. 3. (a) Schematic illustration of band structures and resonant Raman scattering process of InSe. The band-gap transition is marked as A transition, while the electronic transition between the top of the Se-4$p_{x/y}$ orbital band and the bottom of the conduction band (In-5s orbital) is marked as B transition. (b) Normalized PL spectra of a strained 12-layer InSe; the green line is the laser line of 514.5 nm laser (2.41 eV) for Raman measurements and the two gray rectangles correspond to the sharp Raman peaks from the substrate, which we intentionally removed. The spectra are vertically shifted for clarity. (c) The differential reflectance spectra of 1- to 8-layer InSe; the gray triangles denote the absorption peak of exciton B. (d) The layer-dependent energy of exciton B without and with 1.15% uniaxial tensile strain; the data points for 8- to 30-layer InSe come from PL measurements, while the results of 1- to 5-layer InSe are originated from the differential reflectance spectra. The green horizontal line is the photon energy of the 514.5 nm laser (2.41 eV).

section of Raman scattering reads

$$\sigma \cong |W_{\mathrm{fi}}|^2 = \left| \sum_{\alpha} \frac{M_{eR}(\omega_s) M_{ep} M_{eR}(\omega_i)}{(\hbar\omega_s - \hbar\omega_\alpha + i\Gamma)(\hbar\omega_i - \hbar\omega_\alpha + i\Gamma)} \right|^2, \tag{1}$$

where W_{fi} are the matrix elements for Raman scattering, ω_i, ω_s, and ω_α are the frequencies of the incident photon, scattered photon, and electronic intermediate state (the frequency of the first-order phonon is $\omega_0 = \omega_i - \omega_s$ for Stokes Raman scattering), respectively, Γ is the damping factor of the exciton, and M_{eR} and M_{ep} denote the matrix elements for the electron-photon and electron-phonon interactions, respectively.

For selection-rule-allowed phonon modes, the phonon matrix elements M_{ep} are nonvanishing and independent of phonon wave vector q as $q \to 0$. The two denominators account for the enhancement of the Raman cross section in resonance conditions [34]. On the contrary, for the forbidden Raman modes, the phonon matrix element M_{ep} for intraband Fröhlich scattering vanishes at long wavelength ($q \to 0$), so the higher-order term of the wave vector dominates the scattering cross section. The q-dependent matrix element M_{ep} is proportional to qa^2, where a is the energy-dependent characteristic length [24,35]: $a \propto \frac{1}{|\hbar\omega_s - \hbar\omega_\alpha + i\Gamma|^{1/2} + |\hbar\omega_i - \hbar\omega_\alpha + i\Gamma|^{1/2}}$. Therefore, in addition to the enhancement caused by the two denominators in Eq. (1), the forbidden LO phonons exhibit more pronounced enhancement than the allowed modes by the intraband electron-phonon scattering channel. Such effect was also observed in CdS [35,36], InSb [37], and bulk γ-InSe [29,30] previously.

D. Phonon softening of strained InSe

Phonon softening under tensile strain is a common phenomenon in 2D materials [14–19]. As tensile strain is applied, the length of the covalent bonds increases, and consequently the restoring force in the vibrations becomes weaker and the phonon frequency decreases. As shown in Figs. 2(b) and 2(c), except for a tiny shift of the A_1 (Γ_1^2) mode, sizable redshifts of all other phonon modes are observed. The phonon frequency and the corresponding redshift for each phonon mode exhibit no meaningful layer dependence; therefore for simplicity, in Figs. 4(a)–4(e), we only show the evolution of Raman peak positions of A_1 (Γ_1^1), E (Γ_3^3)/E (Γ_3^1)-TO, A_1 (Γ_1^1)-LO, E (Γ_3^1)-LO, and A_1 (Γ_1^3) modes of strained 10–15-layer InSe. Similar data for strained 3–6-layer samples are presented in the SM, Sec. S3 [25]. The shift rates under strain are

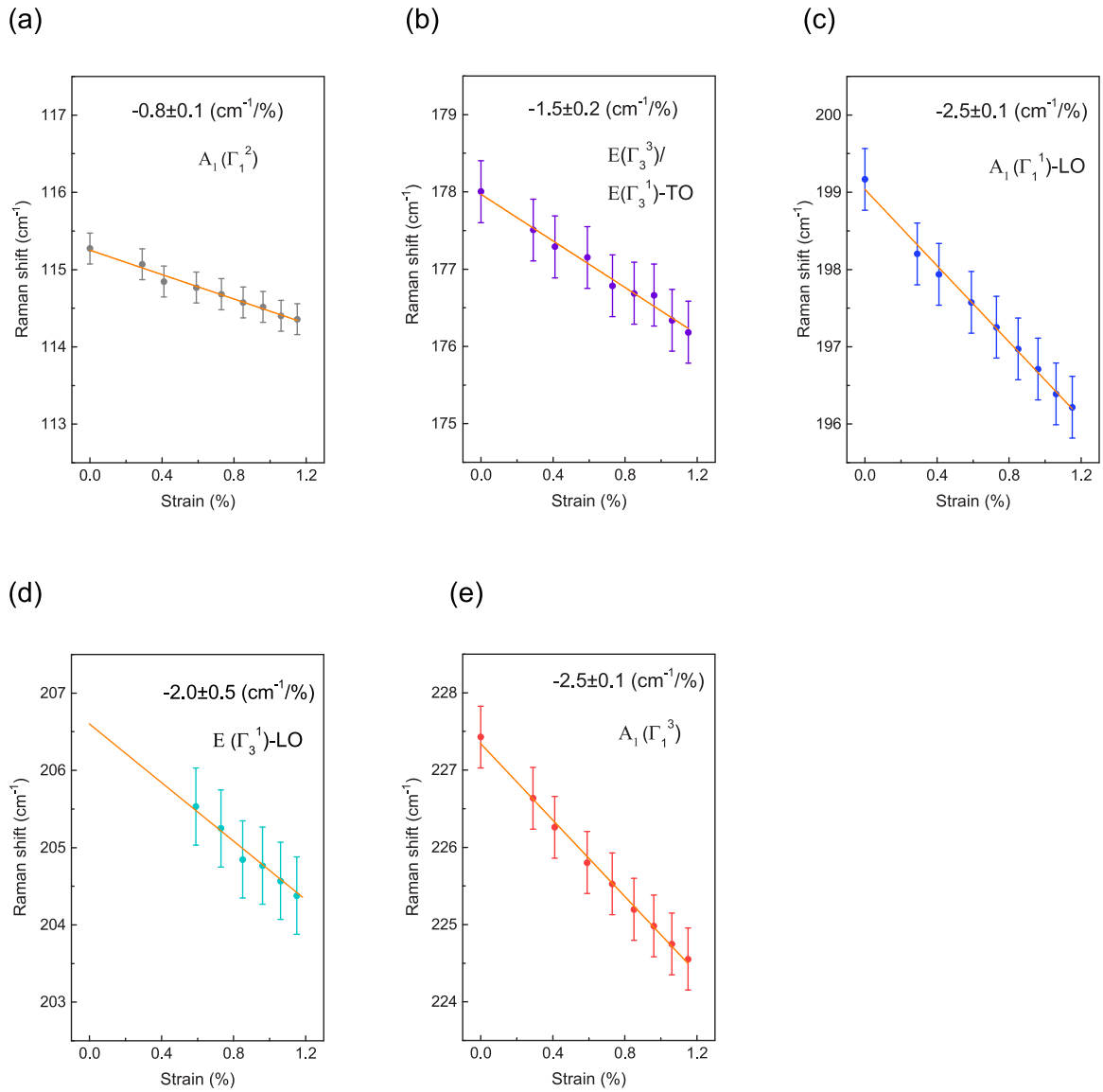

FIG. 4. Evolution of phonon frequencies for 10–15 layer InSe under uniaxial tensile strain. (a)–(e) The A_1 (Γ_1^2), E (Γ_3^3)/E (Γ_3^1)-TO, A_1 (Γ_1^1)-LO, E (Γ_3^1)-LO, and A_1 (Γ_1^3) modes, respectively, in the order of increasing phonon frequency.

summarized in Table I. The shift rates of the A_1 (Γ_1^1)-LO, E (Γ_3^1)-LO, and A_1 (Γ_1^3) modes are much larger than that of the A_1 (Γ_1^2) mode because the A_1 (Γ_1^2) mode is the breathing mode of two In-Se sublayers and in-plane strain has a weaker influence on the atomic vibration in the out-of-plane direction (see SM, Sec. S8 [25]). We performed a first-principles calculation [38–41] to obtain the phonon dispersion of InSe. The uniaxial strain is introduced by expanding the lattice along the zigzag direction (a axis) up to 2% with 0.5% per step, while the same strain along the other (armchair) direction gives similar results. The SM, Sec. S7 [25], shows phonon dispersion of monolayer InSe with and without strain, which confirms that all first-order optical phonon modes exhibit sizable redshifts as uniaxial tensile strain is applied. The calculated shift rates are summarized in Table I, which are consistent with experimental results.

TABLE I. The shift rates (in cm^{-1}/%) of few-layer InSe are based on Raman experiments and monolayer InSe from DFPT calculations. The point group of monolayer InSe is D_{3h}, and the corresponding irreducible representations are denoted.

Mode	3–6 L	10–15 L	Mode	1 L
E (Γ_3^2)			E''	−0.4
A_1 (Γ_1^2)	-0.8 ± 0.1	-0.8 ± 0.1	A_1'	−0.7
E (Γ_3^3)	-1.5 ± 0.2	-1.5 ± 0.1	E''	−1.3
E (Γ_3^1)-TO	-1.5 ± 0.2	-1.5 ± 0.1	E'-TO	−1.4
A_1 (Γ_1^1)-LO	-2.7 ± 0.2	-2.5 ± 0.1	A_2''-LO	−2.5
E (Γ_3^1)-LO		-2.0 ± 0.5	E'-LO	−1.1
A_1 (Γ_1^3)	-2.4 ± 0.2	-2.5 ± 0.1	A_1'	−1.7

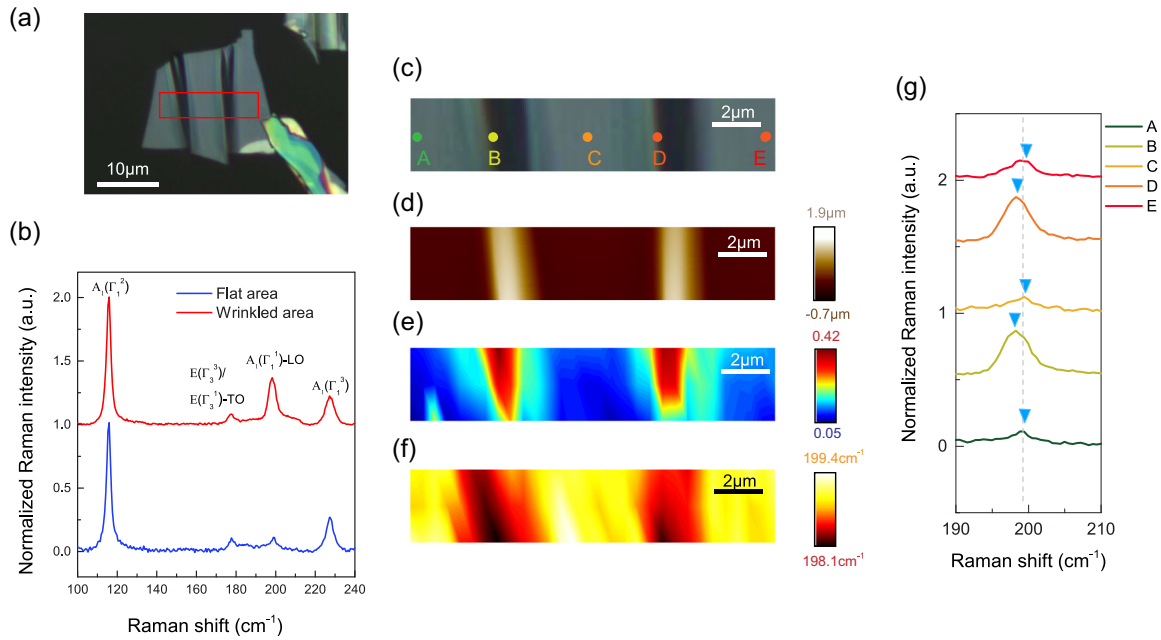

FIG. 5. (a) The microscope optical image of a wrinkled InSe flake (about 15 layers), with the red rectangle denoting the mapping area. (b) The Raman spectra measured on the flat and wrinkled areas. (c) The optical image of wrinkled InSe with two wrinkles; the colored points A to E correspond to different flat and wrinkled areas. (d) The AFM topography image of the sample. (e) The mapping of normalized Raman intensity and (f) peak position of the A_1 (Γ_1^1)-LO phonon mode. (g) The Raman spectra of the A_1 (Γ_1^1)-LO phonon mode for the five points indicated in (c); the blue triangles denote the corresponding Raman peaks and the vertical gray dashed line indicates the peak position of the A_1 (Γ_1^1)-LO phonon mode on a flat area (199.0 cm^{-1}).

E. Strain distribution through Raman mapping

The strong dependence of Raman intensity on strain can be utilized as a sensitive means to determine the spatial variation of strain. As a proof of concept, we mapped the A_1 (Γ_1^1)-LO phonon-mode intensity for a wrinkled sample. We intentionally formed wrinkles in few-layer InSe and induced local uniaxial tensile strain [26,27]. As shown in Figs. 5(a) and 5(c), two wrinkles were created on a 15-layer InSe (see SM, Sec. S10 [25]). AFM topography [see Fig. 5(d)] shows that the height of wrinkles is about 2–3 μm and the width is about 1 μm. According to Figs. 5(b) and 5(g), the normalized Raman intensity of the A_1 (Γ_1^1)-LO phonon mode on the wrinkle is one order of magnitude larger than that in the flat region, indicating a stronger resonance effect on top of the wrinkle. The spatial distribution of normalized Raman intensity is shown in Fig. 5(e). In addition, the strain effect can also be mapped by phonon frequency, as illustrated in Figs. 5(f) and 5(g). The Raman peak of the A_1 (Γ_1^1)-LO phonon mode redshifts by approximately 0.8–1.2 cm^{-1}, and a maximum of 0.3–0.5% strain was induced based on Table I (shift rate $-2.5 \pm 0.1\ \mathrm{cm}^{-1}/\%$). The spatial variation of Raman intensity provides a method to map the strain of 2D materials. Compared to the strain-induced shift of Raman peaks, large intensity contrast can potentially contribute to better mapping sensitivity and contrast for the strain field, if the photon energy is close to the exciton energy. Through the comparison of Figs. 5(d)–5(f), we find that the profile of wrinkles is perfectly mapped by the spatial distribution of Raman intensity, while that obtained from phonon frequency exhibits larger blurring. This is because the Raman intensities of the A_1 (Γ_1^1)-LO phonon mode between the wrinkled and flat areas are distinctively different (an order of magnitude), while the shift of the peak position is small ($<1\ \mathrm{cm}^{-1}$) and demands careful differentiation.

IV. CONCLUSION

In summary, we measured the resonant Raman spectra of few-layer InSe. Large enhancement of phonon modes A_1 (Γ_1^1)-LO and E (Γ_3^1)-LO is observed, which originates from the dominant intraband Fröhlich electron-phonon interactions. Phonon softening is observed in the strained InSe and the shift rates are perfectly consistent with DFPT calculations. The spatial distribution of strain in a wrinkled few-layer InSe is illustrated by mapping the Raman intensity of the forbidden A_1 (Γ_1^1)-LO phonon mode.

ACKNOWLEDGMENTS

H.Y. is grateful for the financial support from the National Young 1000 Talents Plan, National Natural Science Foundation of China (Grants No. 11874009 and No. 11734007), the National Key Research and Development Program of China (Grants No. 2016YFA0203900 and No. 2017YFA0303504), Strategic Priority Research Program of Chinese Academy of Sciences (Grant No. XDB30000000), and the Oriental Scholar Program from the Shanghai Municipal Education Commission. Part of the experimental work was carried out at the Fudan Nanofabrication Laboratory. H.W. is supported by the National Natural Science Foundation of China (Grants No. 11474059 and No. 11674064), and by the

National Key Research and Development Program of China (Grant No. 2016YFA0300700). Z.S. is grateful for the financial support from the National Key Research and Development Program of China (Grants No. 2016YFA0203900 and No. 2017YFA0207303), the National Natural Science Foundation of China (Grant No. 21771040), and the 1000 Plan Program for Young Talents. C.W. is grateful for the financial support from the National Natural Science Foundation of China (Grant No. 11704075) and the China Postdoctoral Science Foundation. G.Z. acknowledges the financial support from the National Natural Science Foundation of China (Grant No. 11804398).

[1] K. S. Novoselov, A. K. Geim, S. V. Morozov, D. Jiang, Y. Zhang, S. V. Dubonos, I. V. Grigorieva, and A. A. Firsov, Science **306**, 666 (2004).
[2] K. F. Mak, C. Lee, J. Hone, J. Shan, and T. F. Heinz, Phys. Rev. Lett. **105**, 136805 (2010).
[3] B. Lalmi, H. Oughaddou, H. Enriquez, A. Kara, S. Vizzini, B. Ealet, and B. Aufray, Appl. Phys. Lett. **97**, 223109 (2010).
[4] F. F. Zhu, W. J. Chen, Y. Xu, C. L. Gao, D. D. Guan, C. H. Liu, D. Qian, S. C. Zhang, and J. F. Jia, Nat. Mater. **14**, 1020 (2015).
[5] L. Li, Y. Yu, G. J. Ye, Q. Ge, X. Ou, H. Wu, D. Feng, X. H. Chen, and Y. Zhang, Nat. Nanotechnol. **9**, 372 (2014).
[6] G. Zhang, S. Huang, A. Chaves, C. Song, V. O. Ozcelik, T. Low, and H. Yan, Nat. Commun. **8**, 14071 (2017).
[7] G. W. Mudd, S. A. Svatek, T. Ren, A. Patanè, O. Makarovsky, L. Eaves, P. H. Beton, Z. D. Kovalyuk, G. V. Lashkarev, Z. R. Kudrynskyi, and A. I. Dmitriev, Adv. Mater. **25**, 5714 (2013).
[8] S. Sucharitakul, N. J. Goble, U. R. Kumar, R. Sankar, Z. A. Bogorad, F. Chou, Y. Chen, and X. P. A. Gao, Nano Lett. **15**, 3815 (2015).
[9] D. A. Bandurin, A. V. Tyurnina, G. L. Yu, A. Mishchenko, V. Zólyomi, S. V. Morozov, R. K. Kumar, R. V. Gorbachev, Z. R. Kudrynskyi, S. Pezzini, Z. D. Kovalyuk, U. Zeitler, K. S. Novoselov, A. Patanè, L. Eaves, I. V. Grigorieva, V. I. Fal'ko, A. K. Geim, and Y. Cao, Nat. Nanotechnol. **12**, 223 (2017).
[10] S. R. Tamalampudi, Y. Y. Lu, K. U. Rajesh, R. Sankar, C. D. Liao, M. B. Karukanara, C. H. Cheng, F. C. Chou, and Y. T. Chen, Nano Lett. **14**, 2800 (2014).
[11] S. Lei, L. Ge, S. Najmaei, A. George, R. Kappera, J. Lou, M. Chhowalla, H. Yamaguchi, G. Gupta, R. Vajtai, A. D. Mohite, and P. M. Ajayan, ACS Nano **8**, 1263 (2014).
[12] Z. Yang, W. Jie, C. H. Mak, S. Lin, H. Lin, X. Yang, F. Yan, S. P. Lau, and J. Hao, ACS Nano **11**, 4225 (2017).
[13] R. Roldán, A. Castellanos-Gomez, E. Cappelluti, and F. Guinea, J. Phys.: Condens. Matter **27**, 313201 (2015).
[14] T. M. G. Mohiuddin, A. Lombardo, R. R. Nair, A. Bonetti, G. Savini, R. Jalil, N. Bonini, D. M. Basko, C. Galiotis, N. Marzari, K. S. Novoselov, A. K. Geim, and A. C. Ferrari, Phys. Rev. B **79**, 205433 (2009).
[15] M. Huang, H. Yan, C. Chen, D. Song, T. F. Heinz, and J. Hone, Proc. Natl. Acad. Sci. USA **106**, 7304 (2009).
[16] H. J. Conley, B. Wang, J. I. Ziegler, R. F. Haglund, S. T. Pantelides, and K. I. Bolotin, Nano Lett. **13**, 3626 (2013).
[17] C. Rice, R. J. Young, R. Zan, U. Bangert, D. Wolverson, T. Georgiou, R. Jalil, and K. S. Novoselov, Phys. Rev. B **87**, 081307(R) (2013).
[18] S. Appalakondaiah, G. Vaitheeswaran, S. Lebègue, N. E. Christensen, and A. Svane, Phys. Rev. B **86**, 035105 (2012).
[19] R. Fei and L. Yang, Appl. Phys. Lett. **105**, 083120 (2014).
[20] S. B. Desai, G. Seol, J. S. Kang, H. Fang, C. Battaglia, R. Kapadia, J. W. Ager, J. Guo, and A. Javey, Nano Lett. **14**, 4592 (2014).
[21] T. Hu, J. Zhou, and J. Dong, Phys. Chem. Chem. Phys. **19**, 21722 (2017).
[22] C. Song, F. Fan, N. Xuan, S. Huang, G. Zhang, C. Wang, Z. Sun, H. Wu, and H. Yan, ACS Appl. Mater. Interfaces **10**, 3994 (2018).
[23] Y. Li, T. Wang, M. Wu, T. Cao, Y. Chen, R. Sankar, R. K. Ulaganathan, F. Chou, C. Wetzel, C. Y. Xu, S. G. Louie, and S. F. Shi, 2D Mater. **5**, 021002 (2018).
[24] R. M. Martin and L. M. Falicov, Resonant Raman Scattering, in *Light Scattering in Solids I*, edited by M. Cardona (Springer, Heidelberg, 1983).
[25] See Supplemental Material at http://link.aps.org/supplemental/10.1103/PhysRevB.99.195414 for optical contrast of few-layer InSe, two-point bending apparatus, the phonon frequencies of strained 3–6 layer InSe, the Raman spectra of strained few-layer InSe with the excitation of a 473 and 532 nm laser, the PL spectra of strained few-layer InSe, calculated phonon dispersion and bond lengths of strained InSe, the resonant Raman spectra of bulklike InSe, wrinkle fabrication setup, excitation wavelength dependence of few-layer InSe, and comparison of the strain effect with and without clamping.
[26] A. Castellanos-Gomez, R. Roldán, E. Cappelluti, M. Buscema, F. Guinea, H. S. J. van der Zant, and G. A. Steele, Nano Lett. **13**, 5361 (2013).
[27] S. Yang, C. Wang, H. Sahin, H. Chen, Y. Li, S.-S. Li, A. Suslu, F. M. Peeters, Q. Liu, J. Li, and S. Tongay, Nano Lett. **15**, 1660 (2015).
[28] N. M. Gasanly, B. M. Yavadov, V. I. Tagirov, and E. A. Vinogradov, Phys. Status Solidi **89**, K43 (1978).
[29] N. Kuroda and Y. Nishina, Solid State Commun. **28**, 439 (1978).
[30] N. Kuroda and Y. Nishina, Solid State Commun. **34**, 481 (1980).
[31] N. Kuroda, I. Munakata, and Y. Nishina, J. Phys. Soc. Jpn. **51**, 839 (1982).
[32] S. J. Magorrian, V. Zólyomi, and V. I. Fal'ko, Phys. Rev. B **94**, 245431 (2016); **96**, 079905(E) (2017).
[33] J. Camassel, P. Merle, H. Mathieu, and A. Chevy, Phys. Rev. B **17**, 4718 (1978).
[34] E. del Corro, H. Terrones, A. Elias, C. Fantini, S. Feng, M. A. Nguyen, T. E. Mallouk, M. Terrones, and M. A. Pimenta, ACS Nano **8**, 9629 (2014).
[35] R. M. Martin, Phys. Rev. B **4**, 3676 (1971).
[36] R. M. Martin and T. C. Damen, Phys. Rev. Lett. **26**, 86 (1971).
[37] W. Dreybrodt, W. Richter, and M. Cardona, Solid State Commun. **11**, 1127 (1972).
[38] R. M. Pick, M. H. Cohen, and R. M. Martin, Phys. Rev. B **1**, 910 (1970).
[39] P. E. Blöchl, Phys. Rev. B **50**, 17953 (1994).
[40] G. Kresse and J. Furthmüller, Phys. Rev. B **54**, 11169 (1996).
[41] A. Togo and I. Tanaka, Scr. Mater **108**, 1 (2015).